Hydrothermal synthesis of porous K^+-containing flower-like delte MnO_2 with high specific capacitance

Li Wang[1], *Hui Wang*[2] ✉

[1]*School of Chemistry and Environmental Engineering, Pingdingshan University, Pingdingshan 467000, People's Republic of China*
[2]*College of Chemistry and Chemical Engineering, Northwest Normal University, Lanzhou 730070, People's Republic of China*
✉ *E-mail: wanghui3931@126.com*

Published in Micro & Nano Letters; Received on 16th April 2017; Accepted on 2nd May 2017

In this study, porous K^+-containing flower-like delte-MnO_2 constructed by numerous thin two-dimensional nanosheets was fabricated by a hydrothermal procedure. Its flower-like morphology was revealed by scanning electron microscopy. The construction units, the ultrathin sheets, were observed from transmission electron microscopy. Its delte-type crystal was characterised via X-ray diffraction. Its porous structure was convinced through N_2 adsorption–desorption isotherms. The properties of delte-MnO_2 nanoflowers as an active electrode constituent for electrochemical capacitors were examined by cyclic voltammetry and galvanostatic charge–discharge in 1 mol l^{-1} Na_2SO_4 electrolyte, and a specific capacitance of 227.2 F g^{-1} was obtained at a current density of 0.05 A g^{-1}. The obtained delte-MnO_2 shows a good long-term stability, suggesting it is a potential electrode material for capacitors.

1. Introduction: Electrochemical capacitors (ECs) were perceived as prospective electrochemical energy storage installations. They have some inherent advantages including high-energy density, speedy charge–discharge rate, wide working temperature range, long cycle life, high safety factor and environmentally benign nature [1]. With features complementary to batteries and fuel cells, ESc have been widely used as energy storage units in many areas, such as smart grids, renewable systems, electric vehicles and fuel cell power systems. The electrochemical performances of ECs depend on the capacitor properties of active electrode material, and thus to exploit new electrode materials for ECs is an efficient approach for improving the performances [2].

Recently, MnO_2 were intensively investigated as a promising electrode material for ECs owing to some advantages, such as abundance, cheapness, high enough theoretical capacitance, as well as eco-friendly nature [3]. MnO_2 is polymorphic with several different crystal structures, whose structural frameworks consist of MnO_6 octahedra sharing vertices and edges. Among the crystal sorts of MnO_2often found, α-, β-, γ-, and ε-, and ρ-MnO_2 possess one-dimensional (1D) channel structures, while δ-MnO_2 has an open 2D layered structure, and λ-MnO_2 has an interconnected 3D networks structure [4]. Brousse and co-workers firstly studied the influence of different crystal structures on capacitive nature of the MnO_2 electrode materials, and found that the capacitance values of MnO_2 with different crystal structures follows the order: 2D tunnel structure >3D tunnel structure >1D tunnel structure [5]. Different crystalline manganese oxides with diverse morphology prepared by Devaraj and Munichandraiah via the aqueous-phase method also confirmed the above result, and the obtained specific capacitance values follow the order: $\alpha > \delta > \varepsilon > \gamma > \lambda$ [6]. When operating temperature varies from about 25 to −35°C, the capacitance of δ-MnO_2–based capacitor was larger than those of α-, β-, and γ- MnO_2–based capacitors [7]. It was also found that sizes of the tunnels in MnO_2 significantly affect the intercalation of cations including H^+, Na^+, K^+, etc. which plays an important role in its supercapacitive storage process [8]. Consequently, many research about the preparation and/or electrochemical nature of MnO_2 supercapacitors are mainly centred upon δ-MnO_2. For instance, capacitance of lamellar birnessite-type MnO_2 prepared by Yan *et al*. via a hydrothermal method was 242.1 F g^{-1} at 2 mA cm^{-2} in 2 mol l^{-1} $(NH_4)_2SO_4$ aqueous electrolyte [9]. Birnessite-type MnO_2 with one-dimensional nanostructures was also prepared by Yu *et al.* through microwave-assisted emulsion method, which showed a high-specific capacitance of 277 F g^{-1} at 0.2 mA cm^{-2} [10].

On the other hand, the performance of MnO_2 capacitors is also affected by the morphology since the capacitive storage process is account of the surface adsorption of electrolyte cations [8]. Then, preparing δ-MnO_2 with unique morphology is beneficial for the usage of MnO_2 materials. For example, flower-like birnessite MnO_2 was prepared by Beaudrouet *et al*. by reduction of $KMnO_4$ in acidic aqueous medium, which displayed a specific capacitance of 75 F g^{-1} at 2 mV s^{-1} of a scan rate [11]. Li *et al.* synthesised flower-like porous birnessite MnO_2 using thermally reduced graphene oxide paper as a sacrificing template achieved an enhanced capacitance of 194 F g^{-1} at 0.1 A g^{-1} [12]. From these reports, the hierarchical flower-like structure is a favourable architecture due to that the structure would offer more interspaces for the mass to diffuse into the inner part of the materials, thus the materials with the hierarchical flower-like structure exhibited a good performance in including many fields such as the sensor of flower-like ZnO [13, 14], catalysis [15] and capacitor [16]. However, the method using the sacrificing template significantly increased the cost of MnO_2 compared with MnO_2 prepared by Beaudrouet *et al*. [11]. In this work, we used hydrothermal method to prepare flower-like δ-MnO_2 with hierarchical structure without using template. The obtained flower-like δ-MnO_2 exhibits a good electrochemical performance with the potential for an active electrode material for ECs.

2. Experimental

2.1. Materials preparation: 20 ml of 0.04 mol l^{-1} $MnSO_4$ solution was added drop-wise to 20 ml of 0.2 mol l^{-1} $KMnO_4$ solution with vigorous stirring. The above solution was topped up to 80 ml with ultra-pure water and then transferred to 100 ml Teflon-lined autoclave, and heated at 140°C for 14 h. After that, the autoclave was gotten to cool to the room temperature. The MnO_2 product was obtained by centrifugation, washed with distilled water and then dried overnight in air at 60°C.

2.2. Characterisation: The crystalline structures of the sample were analysed by X-ray diffraction (XRD, Shimadzu XD-3A (Japan) goniometer, using a Cu Kα radiation operating at 40 kV and 35 mA). The morphologies of the catalyst were analysed using a

doi: 10.1049/mnl.2017.0249

Carl Zeiss Ultra Plus field emission scanning electron microscope (SEM), a transmission electron microscope (TEM) and a JEM-2010 Electron Microscope (Japan) with an acceleration voltage of 200 kV. The specific surface areas were analysed by the Brunauer–Emmett–Teller (BET) method using a Quantachrome Autosorb-1 volumetric analyser. X-ray photoelectron spectrascopy (XPS, Thi-5702 America) was carried out using amonochromatic Al Ka X-ray source to assess the surface composition.

2.3. Electrochemical measurements: The working electrode is prepared via the next procedure. δ-MnO_2, Vulcan carbon and polytetrafluoroethylene with the mass ratio of 80 : 10 : 10 into ethylene glycol were mixed into a uniform serum. Next, the mixture was rolled out to form uniform slices. In vacuum, the slices were dried at 80°C for 6 h. Subsequently, the slices were pressed onto the stainless steel mesh (1 cm^2). The amount of electrode material on the electrode was approximately 10 mg.

A three-electrode cell is adopted for the measurement. The reference electrode is a Hg/Hg_2SO_4 (saturated K_2SO_4) electrode. The counter electrode is a slice of Pt mesh. 1.0 mol l^{-1} Na_2SO_4 is used as the electrolyte. Cyclic voltammograms (CV) and galvanostatic charge/discharge tests are carried out to assess the electrochemical behaviour of δ-MnO_2. CV tests were done in the voltage of between −0.654 V and 0.146 V (0 ~ 0.8 V *vs*. SHE) at different scan rates on a CHI 650D electrochemical workstation. Electrochemical impedance spectroscopy (EIS) were performed between 10 kHz and 0.01 Hz using a 5 mV rms sinusoidal modulation at the open circuit voltage. Galvanostatic charge/discharge test are performed by Neware Battery Tester (Shengzhen Neware Technology Company, China).

3. Results and discussion: The XRD pattern of as-prepared flower-like δ-MnO_2 is presented in Fig. 1*a*. There are four diffraction peaks around 12, 25, 37 and 66° attributed to the hexagonal δ-MnO_2 (JPCDS 86-0666). The crystal structure constructs by 2D edge-sharing MnO_6 octahedral layers inserted with potassium ion and water molecular into the layers' interspace. N_2 adsorption–desorption isotherms of flower-like δ-MnO_2 is present in Fig. 2*b*. The isotherms have the shape of IUPAC-classified IV-type line [17]. A clear hysteresis loop can be seen at the larger relative pressure from 0.48 to 1.0 indicating a relatively large pore size [18], which is also proved by its corresponding pore size distribution. Based on the BET method, the surface area of the flower-like δ-MnO_2 was measured to be 40.4 m^2 g^{-1}. The relatively low specific surface area could be partly attributed to the aggregation of the nanosheets in the hierarchical structure. The total pore volume at 0.995 the relative pressure is 0.32 cm^3 g^{-1}.

Fig. 2*a* displays a large-scaled SEM image of obtained δ-MnO_2, which shows that the δ-MnO_2 are flower-like spheres with diameters of 300–400 nm. High resolution SEM image shown in Fig. 2*b* clearly revealed that the flower-like morphology that are composed of the nano-sheets with the average thickness of about 5–10 nm. This flower-like architecture makes the ions easily arrive the solid/aqueous interface, leading to the increased surface Faradaic and non-Faradaic procedures [11]. Further structural characterisation of flower-like δ-MnO_2 was carried out by TEM. As shown in Fig. 2*c*, the TEM image reveals that the flower-like MnO_2 has a hierarchical architecture which was assembled of many ultrathin 2D nanosheets. The observation is consistent with the SEM result. Compared with the used method in [11] and [12], the flower-like morphology may be result of the nanoflake-assembled effect. During the hydrothermal process, a large number of the nanoflakes were firstly formed. To reduce the surface energy, the nanoflakes tend to gather together, result in the flower-like shape. High magnification TEM displayed in Fig. 2*d* further confirms that the flower-like spheres has open structure with the connected nanosheets with each other which can bring

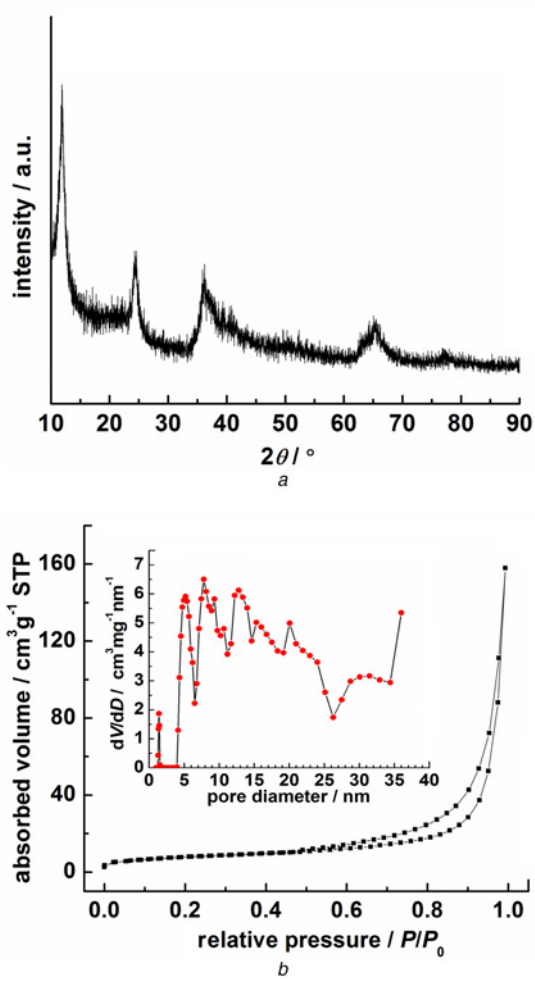

Fig. 1 *XRD pattern of as-prepared flower-like δ-MnO_2*
a XRD pattern
b N_2 adsorption–desorption isotherms of flower-like δ-MnO_2; Inset: the pore size distribution

out abundant space. The collected SAED pattern (Fig. 3*e*) presents multi ring, suggesting that flower-like δ-MnO_2 was polycrystalline. The line-scan EDX spectrum (Fig. 2*g*) indicates the presence of the Mn, K, and O elements, and they are uniformly distributed in the structure.

Electrochemical performance of flower-like δ-MnO_2 was firstly investigated by CV in the potential range from −0.654 to 0.146 V (vs. Hg/Hg_2SO_4). Fig. 3*a* shows CV curves recorded at different scan rates. There is no redox peaks observed in the curves, suggesting the charged–discharged process is through a double-layer mechanism. With the slow scan rate of 2 and 5 mV s^{-1}, the electrode shows a roughly symmetric rectangular shape, which is a typical double-layer capacitive behaviour. With increasing scan rate, the curves' shape departs from the ideal capacitive behaviour. As mentioned above, during the process of the charge storage in MnO_2, the faradic reaction, e.g. the valence conversion of Mn^{4+}/Mn^{3+} occurs, accompanied by the adsorption/desorption of protons (H^+) or alkaline cations (M^+) on the MnO_2 surface, which is likely to be predominant in amorphous MnO_2; or the intercalation/deintercalation of H^+ or M^+ into the MnO_2 structure, which may be predominant in crystalline MnO_2. Since the structure of the obtained flower-like δ-MnO_2 is 2D layered structure, the electrochemical reaction should mainly be the intercalation/deintercalation of Na^+ into the MnO_2 structure coupled with a small faradic reaction. As a negative potential scan potential is applied, the Na^+ ions in the electrolyte will transfer toward the MnO_2 electrode surface.

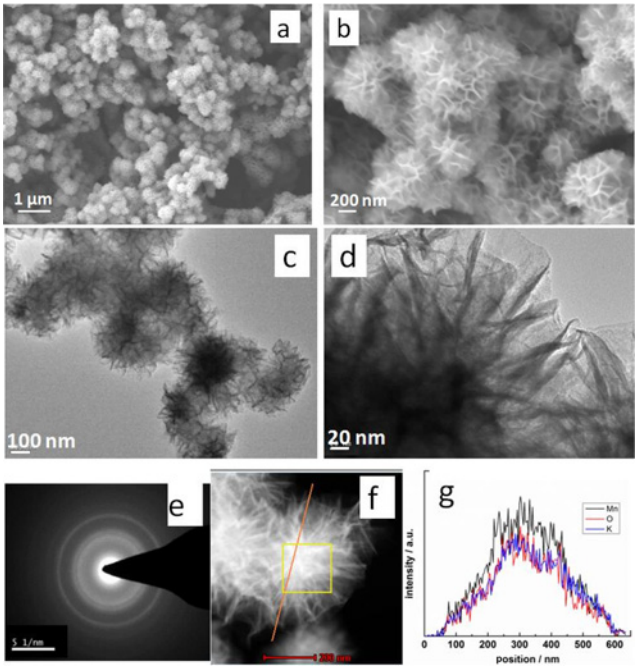

Fig. 2 *N_2 adsorption–desorption isotherms of flower-like δ-MnO_2*
a, *b* SEM images
c, *d* TEM images
e SAED pattern
f STEM image
g line-scan EDX spectrum of δ-MnO_2 nanoflowers

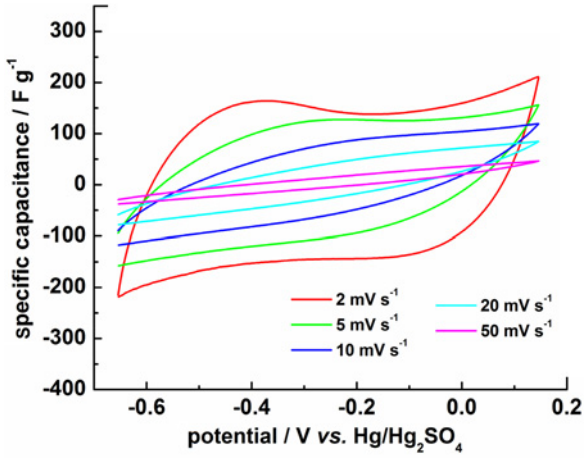

Fig. 3 *Collected CVs*
a CV curves of the flower-like δ-MnO_2 electrode at different scan rates

The following desolvate of the Na^+ ions occurs. Subsequently, the Na^+ ions intercalate into the MnO_2 structure. As the potential is scanned positively, the Na^+ cations deintercalate from the MnO_2structure, and then return into the electrolyte. When a slow rate during the CV process, the Na^+ cations have sufficient time to access toward the δ-MnO_2 electrode surface, neatly being desolvate, hence it is in favour of the intercalation reaction in the 2D layered structure of MnO_2. Thus δ-MnO_2 nanoflowers show good pseudocapacitive behaviour at the slow scan rates. When high-scan rate is used, there are no specific times for the Na^+ cations to intercalate into the MnO_2 structure. This is because the desolvation procedure of Na^+cations is polarised, and consequently leading to the incompletely intercalation into the solid phase [19]. Finally, it is can be seen that the phenomenon of the CV shape being deviated from the ideal rectangular feature.

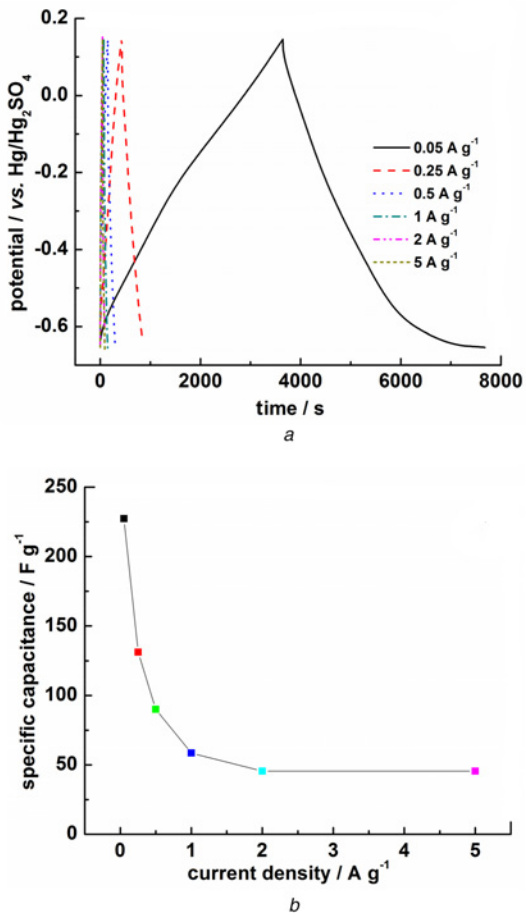

Fig. 4 *Variation of the voltage is close to linear in the whole procedure*
a Charge–discharge behaviour of the flower-like δ-MnO_2 electrode at different current densities
b Variation of specific capacitances at current densities

The capacitor performance of δ-MnO_2 nanoflowers was further studied by galvanostatic charge/discharge technique, which was performed at six regular current densities of 0.05, 0.25, 0.5, 1.0, 2.0 and 5.0 A g^{-1}. As presented in Fig. 4*a*, the variation of the voltage is close to linear in the whole procedure. Meanwhile, the graphical portion during the charge process is almost symmetrical with that of the discharge procedure. These features indicate that the capacitor property of the δ-MnO_2 electrode is mainly derived of the double layer capacitor reaction accompanied with a minor faradaic process [20]. The specific capacitance was calculated from the plots based on the following equation [2]:

$$C(\mathrm{F/g}) = \frac{I\Delta t}{m\Delta V}$$

where I (mA) is the discharge current, Δt (s) is the discharge time, m (mg) represents the mass of the δ-MnO_2 nanoflowers on the electrode, and ΔV (V) is the potential drop during discharge. The variation of the specific capacitances with current densities on the flower-like δ-MnO_2 electrode are plotted in Fig. 4*b*. The specific capacitance at the discharge current density of 0.05 A g^{-1} is 227.2 F g^{-1}. Table 1 summarises some reported results where δ-MnO_2 was applied as electrochemical capacitor electrode materials. As seen in Table 1, the specific capacitance of as-prepared flower-like δ-MnO_2 electrode can be comparable with the electrodes made from other δ-MnO_2, which could be ascribed to its unique structure. One is the 2D layered structure which acts as a succession channel for the diffusion of the electrolyte.

doi: 10.1049/mnl.2017.0249

Table 1 Comparison of the specific capacitance of flower-like δ-MnO_2 electrode to other reported δ-MnO_2 electrodes

Samples	Ref.	C, F g^{-1}	The electrolyte	Scan rate/current density
flower-like δ-MnO_2	This work	227.2	1.0 M Na_2SO_4	0.05 A g^{-1}
		45.5		5 A g^{-1}
K60	[11]	112	0.1 M K_2SO_4	2 mV s^{-1}
The birnessite sample	[21]	176	0.5 M Na_2SO_4	5 mV s^{-1}
δ-MnO_2	[6]	236	0.1 M Na_2SO_4	[a]1 A g^{-1}
Lamellar birnessite-type MnO_2	[9]	242.1	2 M $(NH_4)_2SO_4$	[a]0.26 A g^{-1}
pMHs	[12]	194	1.0 M Na_2SO_4	0.1 A g^{-1}
1D birnessite MnO_2	[10]	277	1.0 M Na_2SO_4	[a]0.71 A g^{-1}

[a]Current density in A g^{-1} is calculated based on the data in literatures.

Another is those interconnected MnO_2 nanosheets which reduces solid-stated transfer distance for the electrolyte into the MnO_2 structure.

The capacitance of the δ-MnO_2 electrode decreases as the increase of the current density. The specific capacitance at the discharge current density of 5 A g^{-1} is 45.5 F g^{-1}. There is only 20% retention of the initial capacitance for the flower-like δ-MnO_2 electrode, indicating its poor rate capability. This maybe because the inner region in the flower-like δ-MnO_2 structure is unreachable for the Na^+ ions at large current density. In addition, compared with the work listed in Table 1, the specific capacitance of flower-like δ-MnO_2 at high current density of 5 A g^{-1} is not high, which is not feasible for practical application. Thus, the rate capability of the as-prepared flower-like δ-MnO_2 should be increased in future.

The cycling life of the flower-like δ-MnO_2 electrode is an index for its applicability. Here, galvanostatic charge/discharge measurement of continuous cycle was carried out. A regular current density of 2 A g^{-1} and a voltage range of −0.654–0.14 V (vs. Hg/Hg_2SO_4) were adopted. A trend between the capacitance retention and the cycle number is present in Fig. 5*a*. As seen, the capacitance retention slightly decreases with increasing of the cycle number, which result of the decrease of the δ-MnO_2 capacitance. After 2000 cycles, the capacitance held 85% of its initial, indicating a good cycling life of the flower-like δ-MnO_2 electrode.

To clear intrinsic reason of the capacitance decrease of the δ-MnO_2 electrode before and after cycling test, EIS was carried out. Typical Nyquist plots are presented in Fig. 6. In high-frequency region, a semicircle appears, which was attributed to the charge transfer process at electrode/electrolyte interface. In low frequency region, a straight line arises, which was ascribed to the ion diffusion process in the bulk of the active mass [22, 23]. As seen, the semicircle becomes larger after cycling test, indicating an increase of charge transfer resistance. Meanwhile, the linear slope decreases after cycling test, suggesting the ion diffusion resistance increases. The increased ion diffusion and charge transfer resistances account for the decrease capacitor performance.

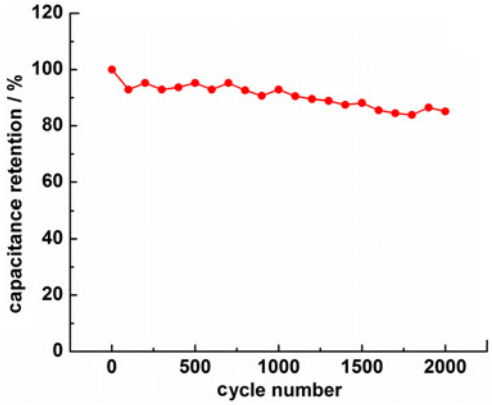

Fig. 5 *Variation between the capacitance retention and the cycle number of the δ-MnO_2 electrode in the 1 mol l^{-1} Na_2SO_4 electrolyte measured using the galvanostatic charge–discharge technique at a current density of 2 A g^{-1}*

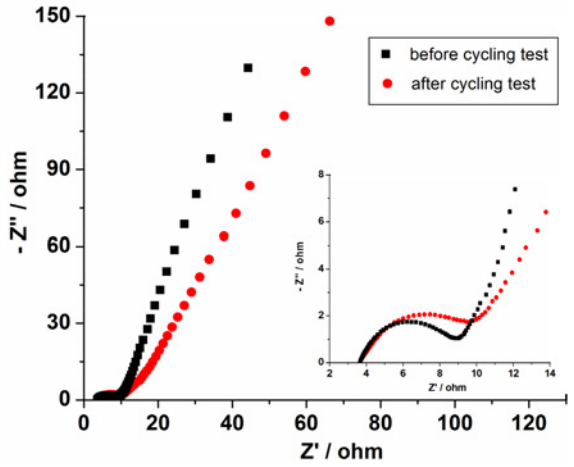

Fig. 6 *Nyquist plots of the EIS for the δ-MnO_2 electrode before and after cycling test. Inset represents the high-frequency region*

As the previous statement, the space between the layers of the δ-MnO_2 structure is affected the intercalation of cations. The change of these cations plays an important role in its supercapacitive storage process. That is to say, the change of inerted K^+ maybe lead to the decrease of the specific capacitance of flower-like δ-MnO_2. To prove the speculation, XPS analysis was performed. As shown in Fig. 7, all the signals are ascribed. Before cycling

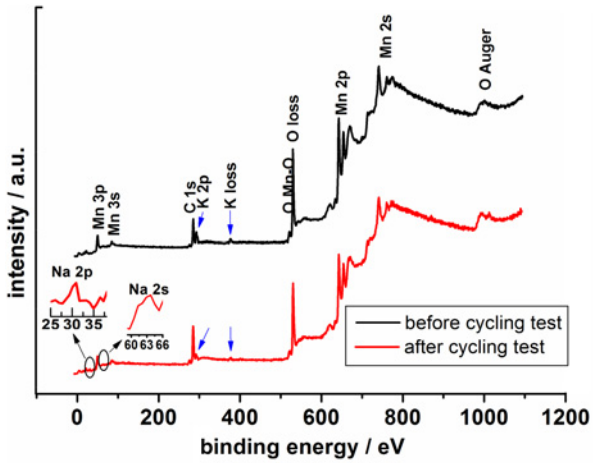

Fig. 7 *XPS survey spectra of the δ-MnO_2before and after cycling test*

test, the K signals clear arise. After cycling test, the *K* signals become very weak, implying its relative content in the δ-MnO_2 structure significantly decreases after cycling test. The result indicates the K^+ loss during the cycling test. Meanwhile, a few of Na^+ substituted the location of K^+, which is proved by the existence of the Na^+ signal presented as the enlarged inserts. These changes maybe make the layer space in the δ-MnO_2 structure shrink. The Na^+ diffusion in the δ-MnO_2 structure becomes difficult, making ion diffusion and charge transfer resistances increase, results in the decrease of the capacitance during cycling test.

4. Conclusion: Porous flower-like δ-MnO_2 spheres were prepared via a hydrothermal route without template. Its flower-like morphology with porous structure was investigated by BET, SEM and TEM. CV curves indicates the capacitance of the δ-MnO_2 electrode mainly originated from the double layer reaction. The flower-like δ-MnO_2 electrode exhibited a high specific capacitance of 227.2 F g^{-1} at a current density of 0.05 A g^{-1}. When increasing the current density, its capacitance decreases because of the incompletely intercalation effect of Na^+ ions. After 2000 cyclic processes, the loss of the specific capacitance was 15%. These results imply that the obtained flower-like δ-MnO_2should be an alternative electrode material for ECs.

5. Acknowledgments: The authors thank the National Natural Science Foundation of China (grant no. 51362027) for financially supporting this work.

6 References

[1] Jiang R., Huang T., Liu J., *ET AL.*: 'A novel method to prepare nanostructured manganese dioxide and its electrochemical properties as a supercapacitor electrode', *Electrochim. Acta*, 2009, **54**, pp. 3047–3052

[2] Wang J.-G., Yang Y., Huang Z.-H., *ET AL.*: 'Interfacial synthesis of mesoporous MnO_2/polyaniline hollow spheres and their application in electrochemical capacitors', *J. Power Sources*, 2012, **204**, pp. 236–243

[3] Li S.-H., Liu Q.-H., Qi L., *ET AL.*: 'Progress in research on manganese dioxide electrode materials for electrochemical capacitors', *Chin. J. Anal. Chem.*, 2012, **40**, pp. 339–346

[4] Wei W., Cui X., Chen W., *ET AL.*: 'Manganese oxide-based materials as electrochemical supercapacitor electrodes', *Chem. Soc. Rev.*, 2011, **40**, pp. 1697–1721

[5] Brousse T., Toupin M., Dugas R., *ET AL.*: 'Crystalline MnO_2 as possible alternatives to amorphous compounds in electrochemical supercapacitors', *J. Electrochem. Soc.*, 2006, **153A**, pp. 2171–A2180

[6] Devaraj S., Munichandraiah N.: 'Effect of crystallographic structure of MnO_2 on its electrochemical capacitance properties', *J. Phys. Chem. C*, 2008, **112**, pp. 4406–4417

[7] Chen L., Li H., Yoshitake H., *ET AL.*: 'Low-temperature performance of aqueous electrochemical capacitors based on manganese oxides', *Electrochim. Acta*, 2015, **157**, pp. 333–344

[8] Yu L.-L., Zhu J.-J., Zhao J.-T.: 'Beta-manganese dioxide nanoflowers self-assembled by ultrathin nanoplates with enhanced supercapacitive performance', *J. Mater. Chem. A*, 2014, **2**, pp. 9353–9358

[9] Yan J., Wei T., Cheng J., *ET AL.*: 'Preparation and electrochemical properties of lamellar MnO_2 for supercapacitors', *Mater. Res. Bull.*, 2010, **45**, pp. 210–215

[10] Yu P., Zhang X., Chen Y., *ET AL.*: 'Preparation and pseudocapacitance of birnessite-type MnO_2 nanostructures via microwave-assisted emulsion method', *Mater. Chem. Phys.*, 2009, **118**, pp. 303–307

[11] Beaudrouet E., Le Gal La Salle A., Guyomard D.: 'Nanostructured manganese dioxides: synthesis and properties as supercapacitor electrode materials', *Electrochim. Acta*, 2009, **54**, pp. 1240–1248

[12] Li Z., Wang J., Wang Z., *ET AL.*: 'Synthesis of a porous birnessite manganese dioxide hierarchical structure using thermally reduced graphene oxide paper as a sacrificing template for supercapacitor application', *New J. Chem.*, 2012, **36**, pp. 1490–1495

[13] Meng F., Ge S., Jia Y., *ET AL.*: 'Interlaced nanoflake-assembled flower-like hierarchical ZnO microspheres prepared by bisolvents and their sensing properties to ethanol', *J. Alloys Compd.*, 2015, **632**, pp. 645–650

[14] Meng F., Hou N., Jin Z., *ET AL.*: 'Sub-ppb detection of acetone using Au-modified flower-like hierarchical ZnO structures', *Sens. Actuators B*, 2015, **219**, pp. 209–217

[15] Ma Y., Wang H., Key J., *ET AL.*: 'Control of CuO nanocrystal morphology from ultrathin 'willow-leaf' to 'flower-shaped' for increased hydrazine oxidation activity', *J. Power Sources*, 2015, **300**, pp. 344–350

[16] Ren Q., Wang R., Wang H., *ET AL.*: 'Ranunculus flower-like $Ni(OH)_2@Mn_2O_3$ as a high specific capacitance cathode material for alkaline supercapacitors', *J. Mater. Chem. A*, 2016, **4**, pp. 7591–7595

[17] Brunauer S., Demine L.S., Deming W.E., *ET AL.*: 'On a theory of the van der Waals adsorption of gases', *J. Am. Chem. Soc.*, 1940, **62**, pp. 1723–1732

[18] Zhou T., Wang H., Ji S., *ET AL.*: 'Soybean-derived mesoporous carbon as an effective catalyst support for electrooxidation of methanol', *J. Power Sources*, 2014, **248**, pp. 427–433

[19] Qu Q., Zhang P., Wang B., *ET AL.*: 'Electrochemical performance of MnO_2 nanorods in neutral aqueous electrolytes as a cathode for asymmetric supercapacitors', *J. Phys. Chem. C*, 2009, **113**, pp. 14020–14027

[20] Sodtipinta J., Pon-On W., Veerasai W., *ET AL.*: 'Chelating agent- and surfactant-assisted synthesis of manganese oxide/carbon nanotube composite for electrochemical capacitors', *Mater. Res. Bull.*, 2013, **48**, pp. 1204–1212

[21] Cormie A., Cross A., Hollenkamp A.F., *ET AL.*: 'Cycle stability of birnessite manganese dioxide for electrochemical capacitors', *Electrochim. Acta*, 2010, **55**, pp. 7470–7478

[22] Wang H., Ren Q., Brett Dan J.L., *ET AL.*: 'Double-shelled tremella-like $NiO@Co_3O_4@MnO_2$ as a high-performance cathod material for alkaline supercapacitors', *J. Power Sources*, 2017, **343**, pp. 76–82

[23] Ji S., Ma Y., Wang H., *ET AL.*: 'Cage-like MnO_2-Mn_2O_3 hollow spheres with high specific capacitance and high rate capability as supercapacitor material', *Electrochim. Acta*, 2016, **219**, pp. 540–546

doi: 10.1049/mnl.2017.0249